Received: 6 June 2020 | Revised: 22 July 2020 | Accepted: 22 July 2020

DOI: 10.1002/eom2.12046

RESEARCH ARTICLE

EcoMat FUNCTIONAL MATERIALS FOR GREEN ENERGY AND ENVIRONMENT WILEY

Surfactant-directed Pd-nanoparticle assemblies as efficient nanoreactors for water remediation

Binbin Huang[1] | **Qianqian Xie**[1] | **Zhan Yang**[1] | **Chao Lei**[2] | **Wenqian Chen**[3] | **Xiang Tang**[1] | **Flavio Maran**[4,5]

[1]College of Environmental Science and Engineering, Hunan University, Changsha, China

[2]School of Hydraulic Engineering, Changsha University of Science and Technology, Changsha, China

[3]Department of Chemical Engineering and Technology, Imperial College London, London, UK

[4]Department of Chemistry, University of Padova, Padova, Italy

[5]Department of Chemistry, University of Connecticut, Storrs, Connecticut

Correspondence
Binbin Huang, College of Environmental Science and Engineering, Hunan University, Changsha 410082, China.
Email: binbinhuang@hnu.edu.cn

Flavio Maran, Department of Chemistry, University of Padova, Via Marzolo, 1, 35131 Padova, Italy.
Email: flavio.maran@unipd.it

Funding information
Hunan Provincial Science and Technology Department, Grant/Award Number: 2018SK2025; National Natural Science Foundation of China, Grant/Award Numbers: 51408209, 51509021, 5177091149

Abstract

Devising new catalytic systems for the efficient removal of organic chlorides from contaminated sites has important benefits for the human health. Efficiency requires the use of performing catalysts and the extraction of the contaminant from the environment. Here we describe a novel strategy that combines both aspects. A one-pot surfactant-directed approach allows the preparation of ultrafine palladium nanoparticles (PdNPs) finely dispersed inside well-ordered geometric structures, ranging from loose vesicles to nanocubes, from cylindrical to spherical assemblies. These assemblies work as nanoreactors where hydrophobic organic chlorides can be concentrated in the surfactant-tail environment and efficiently reduced by the PdNP catalysts. As a proof-of-concept, we studied the dechlorination of the notorious pollutant 4-chlorophenol. The nanoreactors display rapid dechlorination ability, excellent catalytic activity, and good stability and recyclability. This study provides a new methodology for effective water remediation that combines the advantages of both extraction and supported heterogeneous catalysis.

KEYWORDS

catalytic dechlorination, nanoreactor, Pd nanoparticles, surfactant assembly, water remediation

1 | INTRODUCTION

Noble metal nanoparticles (NPs) exhibit physical and chemical properties that are of value in applied catalysis, such as in chemical industrial processes, environment protection, and energy production.[1-5] The catalytic properties of nanomaterials strongly depend on their size, shape, structure, and morphology.[1,2] NPs with high surface-to-volume ratios are especially interesting because they are rich of surface features (edge and corner atoms) that are

Qianqian Xie and Zhan Yang contributed equally to this study.

beneficial to catalysis. In particular, palladium NPs (PdNPs) exhibit useful catalytic properties in several processes, such as the oxidation of fuels, carbon-carbon coupling reactions, alkynes hydrogenation, and dehalogenation of organic chlorides.[1-3,6-8] Their performance and stability, however, are often compromised by aggregation phenomena, and therefore, devising new strategies suitable to avoid these problems is a priority research area.[4,5,8-15]

High-molecular-weight organic compounds like surfactants, polymers, and metal-organic frameworks can be used as soft templates to obtain size- and shape-controlled nanomaterials.[4,5,12-14] Self-assembly of surfactants provides a particularly useful way to prepare well-ordered and ultrafine nanomaterials.[2,5,12,15] Because of their functional groups and ionic properties, surfactants provide useful sorption sites for metal precursors, may induce particles assembly, and generally lead to the formation of highly dispersed and stable metal NPs.[16-18] In addition to stabilizing the metal NPs, the surfactant ligands may induce specific physicochemical properties to the NPs,[8,19] thereby influencing the nanomaterials' solubility and catalytic properties.[8,20,21] For instance, Albuquerque et al used water-soluble polymer-surfactant PdNPs for the hydrogenation of alkenes and α,β-unsaturated ketones.[21] The catalytic efficiency was attributed to a dynamic effect of the protective layer in facilitating the access of substrates onto Pd surface. On the other hand, strongly and heavily adsorbed surfactants may also block the active sites of the metal NP surface with the result of decreasing the catalytic activity.[5,22] The challenge is, therefore, to devise synthetic strategies suitable to optimize benefits and minimize drawbacks of the use surfactants for making and assembling PdNPs.

Here, we describe a facile one-pot method that allows preparing well-ordered PdNPs assemblies and their successful use for the dechlorination of 4-chlorophenol (4-CP). The choice of 4-CP4-CP as the proof-of-concept dechlorination target is because chlorophenols (CPs) are listed as priority environmental pollutants by both China and the US Environmental Protection Agency owing to their strong toxicity and even carcinogenic activity.[23,24] Once released into the ground and surface waters, CPs transfer and accumulate into the surrounding ecosystems, and this constitutes a severe threat for the environment and human health particularly because of their persistence and strong resistance to biodegradation.[25] Developing effective technologies for the removal of organic chlorides is indeed one of the most active topics in the environment field.[25-31] Because it is the halogenated group that makes organic chlorides more toxic and recalcitrant to degradation,[20,31] the goal is to devise effective dehalogenation methods. In this context, nanoscale zero-valent-iron (nZVI) materials, including iron-based bimetallic NPs, have been of particular value due to their low redox potentials and large surface area.[25,31-34] Catalysts based on Ni, Cu, Al, and Pd loaded nZVI have been also shown to perform nicely.[25,31-34] Conceivably, ultrafine nanocatalysts may significantly enhance dechlorination processes, although specific investigations are limited.[35,36] Organic chlorides, such as CPs, are generally hydrophobic and this makes them stably sorbed in the aquifers and soils, or exist as nonaqueous liquid phases.[37] Their degradation requires extraction into the aqueous phase, which can be accomplished by using surfactants or cosolvents.[37] These procedures, however, leave the organic contaminants unaltered, and therefore, further chemical or biological treatments are required. A winning remediation strategy should combine the advantages of surfactants as both supports for the metal NPs and, owing to their hydrophobic tails, solubilizers for the hydrophobic CPs. So far, however, successful preparation and performance test of these materials have not been achieved. In particular, there are few reports regarding the possible synergistic effect between PdNPs and their support.

In this work, we describe a novel approach, based on assembling surfactant/metal NP nanoreactors, with the goal of contributing an alternative strategy for the effective removal of halogenated pollutants from contaminated sites. The preparation of stable nanoreactors, their possible formation mechanisms, properties, and environment implications are described. The strength of this approach lies in a methodology that takes advantage of surfactant assembly to make ultrafine PdNP-decorated nanoreactors, solvent washing, and dehalogenation heterogeneous nanocatalysis. As a proof-of-concept, the so-devised nanoreactor strategy is successfully tested by studying the dechlorination of 4-CP. The mechanism and driving force for the surfactant-directed assembly of PdNPs are also investigated.

2 | RESULTS AND DISCUSSION

2.1 | Synthesis and characterization of PdNPs assemblies

2.1.1 | Preparation of PdNPs assemblies

The electrostatic interaction between anionic inorganic species and cationic surfactants allows achieving a good dispersity and high stability of organometallic complexes. We used cetyltrimethylammonium bromide (CTAB) as the surfactant. The interaction of CTAB with the Pd precursor ($PdCl_4^{2-}$) was studied with ultraviolet-visible (UV-vis) absorption spectroscopy. Figure 1A shows that $PdCl_4^{2-}$ exhibits two absorption peaks at 207 and 237 nm. Upon

addition of CTAB to form a 0.125 mM solution, these peaks shift to 237 and 277 nm, respectively, and the absorption intensity decreases. The red shift undergone by both peaks is attributed to the interaction between CTA^+ and $PdCl_4^{2-}$. We noted that upon addition of CTAB, suspended light-red flocks appear in solution, which can explain the decrease in intensity of the absorption peaks as well as confirm the formation of organometallic complexes. Similar phenomena were previously observed by mixing $PdCl_4^{2-}$ and cetylmethylammonium chloride, with newly formed absorption bands at 226 and 285 nm.[2] The main difference between the two reactions is thus the extent of red shift undergone by the two peaks. Increasing the concentration of CTAB to 1.0 mM (Figure 1A) causes a further red shift of both absorption peaks, to 245 and 327 nm, and an increase in absorption intensity. As the stability constant of $PdBr_4^{2-}$ is about 10^4 times larger than that of $PdCl_4^{2-}$,[38] these observations are attributed to a halide-exchange transformation of the Pd precursor from a tetrachloro- to a tetrabromo-complex (see below). This hypothesis was confirmed by mixing $PdCl_4^{2-}$ directly with KBr and following the progressive replacement of chloride with bromide via UV-vis absorption spectroscopy. Addition of enough KBr indeed causes a significant red shift of both absorption peaks to 250 and 330 nm (Figure 1A), that is, values corresponding to those of $PdBr_4^{2-}$.[38] Beside promoting halide exchange, when the concentration of CTAB exceeds or is near the CMC value (critical micelle concentration, 0.9 mM),[5] surfactant self-assembly leads to the formation of spherical or cylindrical micelles,[2,38] which would cause embedding of the Pd precursors. Incorporation of the Pd precursor into the CTAB micelle decreases repulsion among the positively charged heads of CTA^+ with the consequence of causing reconstruction of the surfactant assembly (see below).

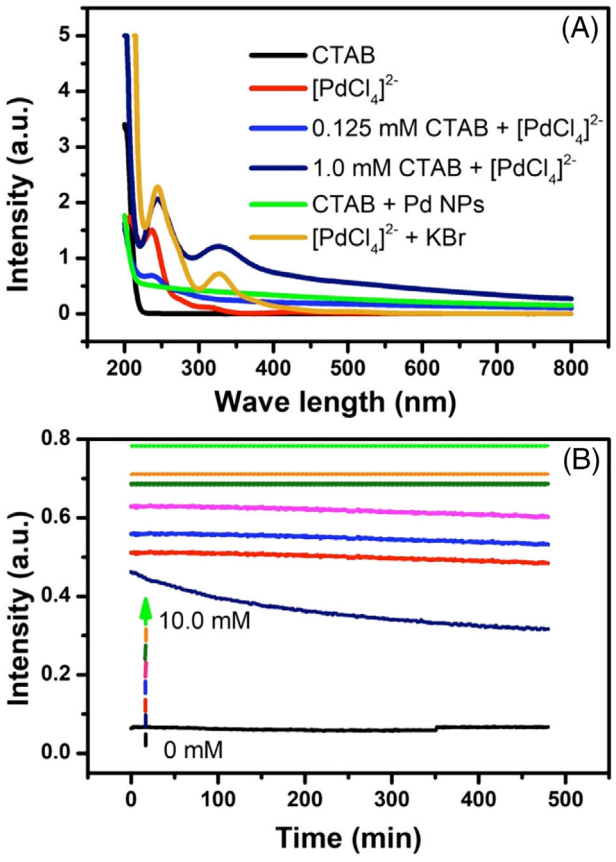

FIGURE 1 A, Ultraviolet-visible (UV-vis) absorption spectra of solutions of cetyltrimethylammonium bromide (CTAB), $PdCl_4^{2-}$, CTAB + $PdCl_4^{2-}$, and CTAB + KBr, as indicated in the legends. B, Sedimentation of palladium nanoparticles (PdNPs) prepared starting from CTAB concentrations of (bottom to top) 0, 0.05, 0.125, 0.25, 0.50, 1.0, 2.0, and 10.0 mM

Upon addition of $NaBH_4$ to the so-formed Pd precursor, the solution turns immediately black, which indicates formation of PdNPs. Thereafter, the growth of PdNPs is mainly directed by the surfactant assembly. Eventually, the aforementioned absorption peaks totally disappear (Figure 1A), pointing to completion of the PdNP synthesis. To gain insights into the stability of the resulting PdNPs assemblies, we followed the progressive sedimentation of PdNPs via UV-vis spectroscopy by setting the wavelength at 237 nm. The sedimentation curves (Figure 1B) indicate that the PdNPs prepared in the presence of CTAB are indeed very stable, especially for concentrations of 0.125 mM or larger, with no obvious change in the absorption intensity even after 24 hours. The results also show a general increase in the adsorption intensity with the CTAB concentration, suggesting an enhanced dispersity and stability of the PdNPs. By contrast, in the absence of CTAB, the PdNPs undergo fast aggregation and sedimentation, which indicates poor stability. The electrostatic interaction between CTA^+ and Pd species is indeed important in both stabilizing the formed PdNPs and inducing surfactant assembly (details are provided in Supporting Information).

2.1.2 | Characterization of the PdNPs assemblies

The PdNPs were characterized by high-resolution transmission electron microscopy-energy-dispersive X-ray spectroscopy (TEM-EDS), scanning electron microscope (SEM), X-ray photoelectron spectroscopy (XPS), and Fourier transform infrared spectra (FTIR). For reference, Figure S1A-C shows the CTAB assemblies obtained at various concentrations in the absence of the Pd precursor. With the exception of 0.125 mM CTAB, which is soluble at this concentration, for larger CTAB concentrations evident spherical micelles with diameters

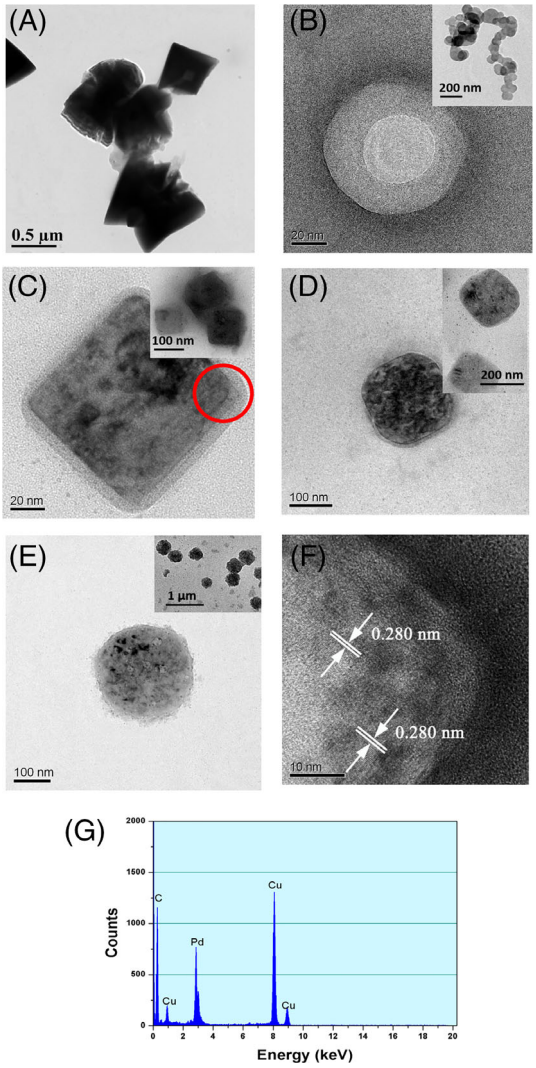

FIGURE 2 Characterizations of the palladium nanoparticles (PdNPs) assemblies. Transmission electron microscopy (TEM) images of Pd particles prepared, A, in the absence of cetyltrimethylammonium bromide (CTAB) or in the presence of, B, 0.125, C, 1.0, D, 2.0, E, 10.0 mM CTAB; the insets to the images of panels (B-E) show images at a smaller magnification. F, HRTEM image of PdNPs (further images are provided in the Supporting Information) prepared in the presence of 1.0 mM CTAB; the inset highlights the crystallinity of the PdNPs, with resolvable atomic lattice. G, Energy-dispersive X-ray spectroscopy (EDS) spectrum corresponding to the zone highlighted by the red circle in (C)

of about 2 nm are observed; no larger assemblies are observed. Figure 2 shows some TEM images of the PdNPs obtained under different conditions. The PdNPs prepared in the absence of CTAB aggregate to form large blocks (Figure 2A), which is attributed to attractions between individual PdNPs.[39] In the presence of CTAB at concentrations lower than the CMC, such as 0.125 mM, a loose vesicle may form primarily due to the van der Waals interactions between the CTAB tails.[16] Figure 2B shows

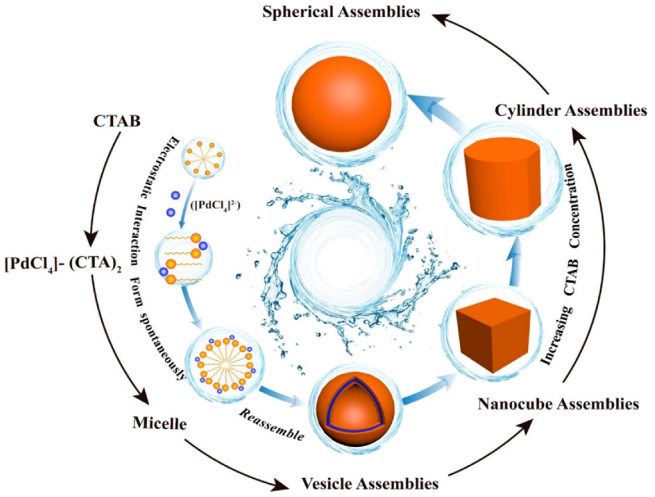

FIGURE 3 Schematic representation of the cetyltrimethylammonium bromide (CTAB)-concentration-dependent production of different palladium nanoparticles (PdNPs) assemblies

the vesicle structure of the CTA^+-Pd complexes (typical diameter of ca. 85 nm). Upon addition of $NaBH_4$, the PdNPs form at both the inner and outer vesicle surfaces, with concomitant disappearance of absorption peaks of the Pd precursor and formation of dark particles in the solution, as monitored by UV-vis absorption spectroscopy (Figure 1A). The effect of the CTAB concentration on the type of aggregate is noteworthy. At 1.0 mM concentration, which already exceeds the CMC value of 0.9 mM, the formation of spherical or cylindrical micelles should be observed.[2] Instead, we observe the formation of nanocube assemblies with a size of ~100 nm (Figure 2C). Increasing the surfactant concentration to 2.0 mM yields an approximately cylindrical structure, with a base's diameter of ~170 nm (Figure 2D). When the CTAB concentration reaches 10.0 mM, the PdNPs assemblies tend to form spherical structures (Figure 2E). The SEM images shown in Figure S1D-G validate the quite uniform features of the PdNPs assemblies obtained at different CTAB concentrations. We attribute the formation of these different structures to the reassembly of the spherical micelle based on the CTA^+-Pd complexes.

Figure 3 provides a pictorial illustration of the above findings. Briefly, there are three structure levels for the formation of well-ordered PdNPs assemblies. Initially, spherical micelles form by van der Waals interactions between surfactant molecules. The second structure level is attributed to the electrostatic interaction between the cationic surfactant and the anionic Pd precursor. The third structure is built on the second structure to form the Pd-nanocube assemblies or some other geometric morphology. Indeed, similar observations of self-assembly of

amphiphilic hyperbranched polymers from unimolecular micelles into big micelles have been previously described, and attributed to intermicellar interactions causing the formation of multimolecular micelles from small micelles.[40-42] The TEM images in Figure 2 reveal the presence of small spheres inside the well-ordered PdNPs assemblies, and this provides some evidence that the former may indeed provide the basic building blocks for formation of the latter. In this process, the driving force mainly comes from the effect brought about by the PdNP assembly in minimizing the electrostatic repulsion between the head groups of the surfactants.[15] The well-ordered architectures directed by the surfactant assembly are presumed to be preserved during the reduction of Pd precursors, as already shown.[2] The presence of the PdNPs in the assemblies are clearly observed in the HRTEM image shown in Figure 2F, in which the inset evidences a distance of 0.231 nm between the two nearest atom rows, as expected for the (111) lattice spacing of face-centered cubic Pd crystals.[3,12,43,44] The PdNPs have an average size of about 5 nm (details are provided in the Supporting Information). The EDS composition analysis further confirms the presence of Pd in the as-obtained assemblies (Figure 2E); Cu originates from the Cu grids used in TEM.

The formation of different PdNPs assemblies is attributed to the surfactant-directed synthesis. Analysis of the nanocube assembly, taken as an example, provides insights into this aspect. Evidence for the presence of CTAB and its interaction with PdNPs were obtained by XPS and FTIR measurements. Figure 4 shows the XPS spectra of both the survey and high-resolution scans for key elements of the PdNPs assemblies. The binding energy (BE) values were calibrated with respect to the C1s peak at 285.0 eV. The XPS survey (Figure 4A) shows peaks corresponding to the BEs of C1s, Br3d, Pd3d, and N1s, which confirm the presence of CTAB-PdNPs complexes in the particles. The atomic percentages are 92.86%, 1.82%, 0.51%, and 4.81%, respectively. The low percentage of Pd (given the experimental conditions, the theoretical atomic percentage of Pd should be 3.52%) suggests that the PdNPs as mainly embedded inside the assemblies, as XPS probes atoms near surface region (within about 5 nm). In Figure 4B, the Pd3d spectrum of the PdNPs assemblies exhibits two individual peaks at 337.08 and 342.25 eV, which are assigned to the BEs of 3d3/2 and 3d5/2 of Pd(0), respectively, suggesting the successful formation of PdNPs from its precursors, in keeping with the TEM results. The BE for N1s in pure CTAB is 398.4 eV, whereas in the PdNPs assemblies the

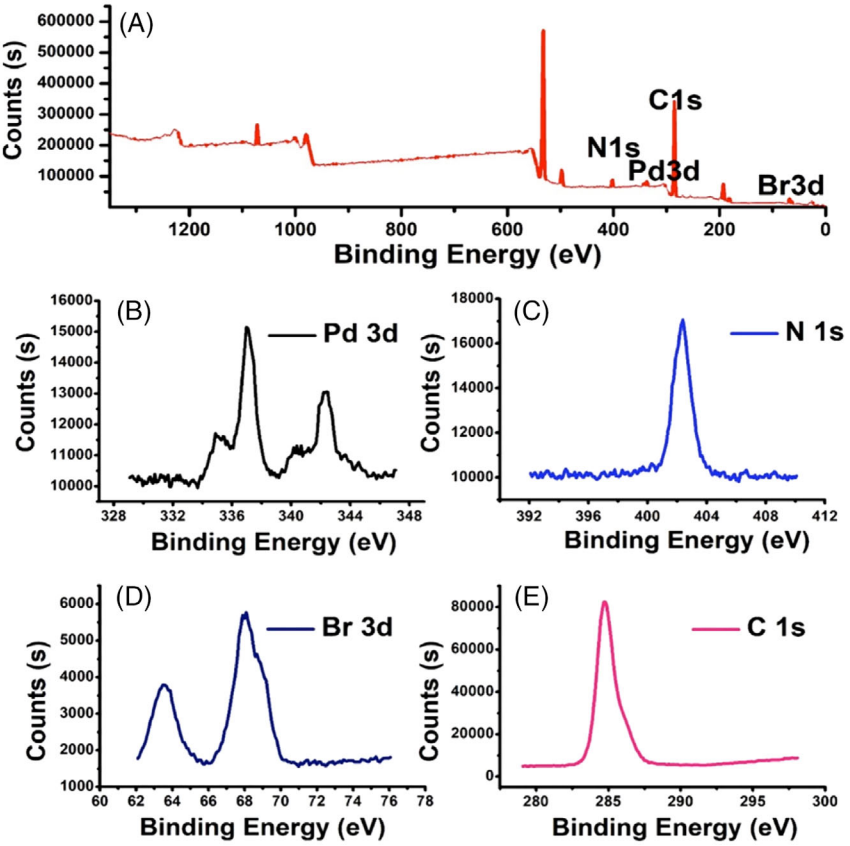

FIGURE 4 (A) X-ray photoelectron spectroscopy (XPS) spectra of survey scan for palladium nanoparticles (PdNPs) assemblies and high-resolution scan of, B, Pd3d, C, N 1s, D, Br3d, and E, C 1s. Note: The PdNPs assemblies were prepared in the presence of 1.0 mM cetyltrimethylammonium bromide (CTAB)

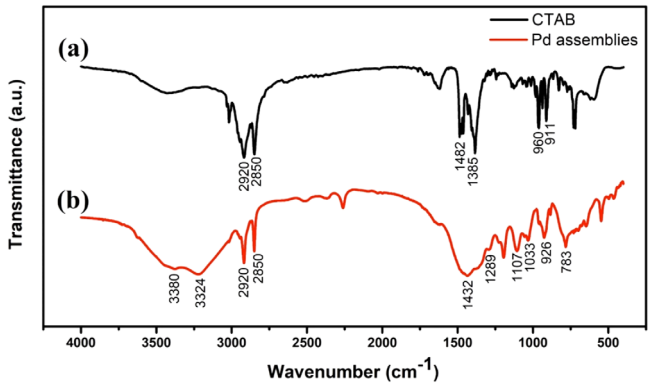

FIGURE 5 Fourier transform infrared spectra (FTIR) spectra of, A, pristine cetyltrimethylammonium bromide (CTAB) and, B, palladium nanoparticles (PdNPs) assemblies prepared in the presence of 1.0 mM CTAB

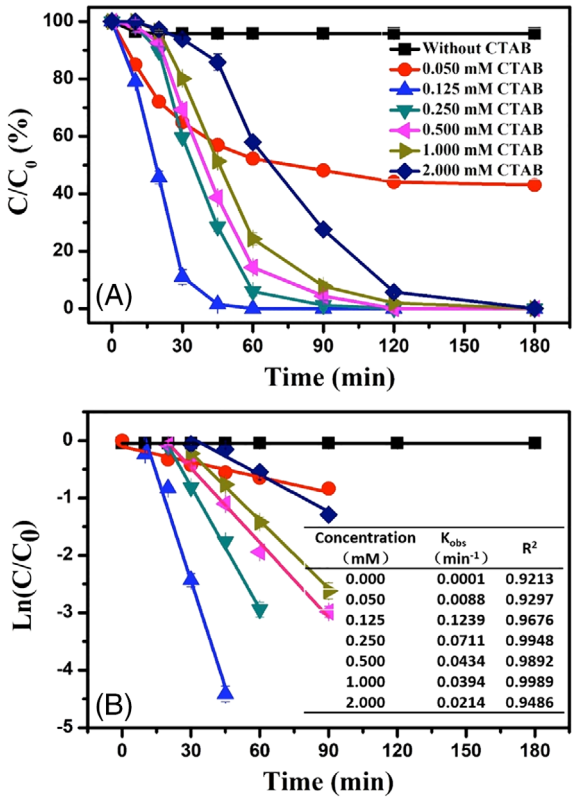

FIGURE 6 Catalytic activity of the palladium nanoparticles (PdNPs) assemblies. Effects of the cetyltrimethylammonium bromide (CTAB) dosage concentration on, A, the dechlorination of 4-chlorophenol (4-CP), in which C/C_0 indicates the ration between the concentrations of 4-CP at the given time and at $t = 0$, and B, the dechlorination rate constants. Reaction conditions: pH 2.0, 25°C, 800 rpm, 1.0 mM 4-CP, 15 mM $NaBH_4$, 12.5 mol% Pd (with respect to 4-CP)

BE is slightly shifted toward the higher value of 402.4 eV, which points to a strong interaction of Pd with the ammonium cation in the formed assemblies.[5] The Br3d peaks at 63.6 and 68.0 eV are attributed to PdX_4^{2-} and CTAB. The C1s spectrum of the PdNPs assemblies has a main band at 285.0 eV, which is due to the C-H bonds in CTAB.[45]

Figure 5 shows the FTIR spectra of pristine CTAB and the PdNPs assemblies. The C-H symmetric and asymmetric vibration frequency modes are found at 2850 and 2920 cm^{-1}, which are the typical vibrational frequencies of pure CTAB.[46,47] The features at about 1482 and 1385 cm^{-1} mainly arise due to the C—H scissoring vibrations of CH_3—N and the C—N stretch vibrations of the CTAB molecule, respectively.[48,49] In the PdNPs assemblies, both peaks are slightly blue shifted to 1432 and 1289 cm^{-1}, respectively, in keeping with the XPS results that point to a strong interaction between Pd and CTAB. The FTIR spectrum also shows two wide vibration bands at about 3380 and 3224 cm^{-1}, which are attributed to the stretch of the hydrogen bonded O—H groups, which points to interactions between surfactant ligands and water in the PdNPs assemblies.[48,50] Compared to pristine CTAB, the absence of the bands at 960 and 911 cm^{-1} and the presence of new peaks at 1107, 1033, 926, and 783 cm^{-1} in the PdNPs assemblies, which are attributed to the stretching modes of C—N^+ effected by the Pd surface,[46,49,51] suggest that the binding of CTAB with PdNPs occurs via the linkage of CTA$^+$(N^+)-Pd (see Supporting Information).[46,51] Similar changes of the vibration-frequency bands upon surfactant modification were also observed in the production of CTAB-decorated AuNPs, supporting the presence of CTAB capping in the nanomaterials.[47,49] Overall, these results further support the notion that CTAB plays a vital role in determining the formation of well-ordered PdNPs assemblies.

2.2 | Catalytic dechlorination of 4-CP

To investigate their catalytic activity, the PdNPs assemblies were tested in the dechlorination of 4-CP to phenol. The reaction was performed with a molar ratio of 4-CP to Pd to $NaBH_4$ of 1:0.125:15. The results (Figure 6) show that excellent dechlorination performances can be achieved with all assemblies prepared. Of the various structures, the loose vesicle assembly, prepared in the presence of 0.125 mM CTAB, exhibits the best outcomes, as 4-CP was quantitatively dechlorinated to phenol within 45 minutes. Instead, the PdNPs prepared in the absence of surfactant only allow very limited conversion (ca. 4% of dechlorination efficiency in 3 hours), which is in keeping with the obvious aggregation phenomena occurring immediately after NP preparation. These results thus demonstrate that the presence of CTAB during the preparation of PdNPs enhances very significantly the dechlorination performance. They also show that the surfactant concentration used to prepare the various assemblies play an important

role in determining the catalysis kinetics, though the efficiency remains virtually unaltered. It should be stressed that phenol was the only hydrohalogenation product, and the selectivity was always 100%.

As aforementioned, CTAB stabilizes the Pd nanocatalyst by electrostatic interactions; thereby, preventing aggregation of the ultrafine PdNPs embedded inside the surfactant assemblies. The organic part of the surfactant is also expected to favor solubilization of hydrophobic substances in water environments, thereby facilitating their access onto the Pd surface. These assemblies can thus be seen as efficient nanoreactors consisting of Pd catalysts and a hydrophobic nanoenvironment concentrating 4-CP. As the CTAB concentration increases, the architecture of the PdNPs assemblies changes progressively from loose vesicle, to the packed nanocube, to the spherical structure (cf. Figure 3). During this transformation, the surfactants get more densely packed and the PdNPs become more embedded inside the now more crowded assemblies. Thus, whereas a high concentration of CTAB enhances stability, it also diminishes the number of active sites on the catalyst surface,[5] which may impair the catalytic activity of PdNPs toward the dechlorination reaction. It thus appears that there is an optimum CTAB concentration providing a compromise between PdNPs' stability and catalytic activity: below 0.125 mM, the PdNPs are less stable and tend to aggregate with each other, whereas at higher concentrations 4-CP is dechlorinated less efficiently because of the reduced number of available/accessible Pd sites.

Figure 6 also shows that there is a clear reaction delay, which is especially evident at higher surfactant concentrations (ca. 30 minutes). This can be attributed to a limited mass transport rate: at the initial reaction stage, hydrogen evolution resulting from rapid hydrolysis of $NaBH_4$ is quite vigorous[3] and this may hinder the diffusion of 4-CP. The presence of more tightly packed surfactant chains on the PdNPs is also expected to slow the diffusion of 4-CP. Eventually, the relative mass-transport processes and surface concentrations allow for optimum reduction of 4-CP, though the rate is still lower (cf. Figure 6B) for the nanoreactors prepared at higher surfactant concentrations. Overall, the PdNPs assemblies exhibit excellent dechlorination activity toward 4-CP reduction, with the PdNPs prepared from 0.125 mM CTAB exhibiting the best catalytic performance. In the following, we will thus focus on this specific nanoreactor.

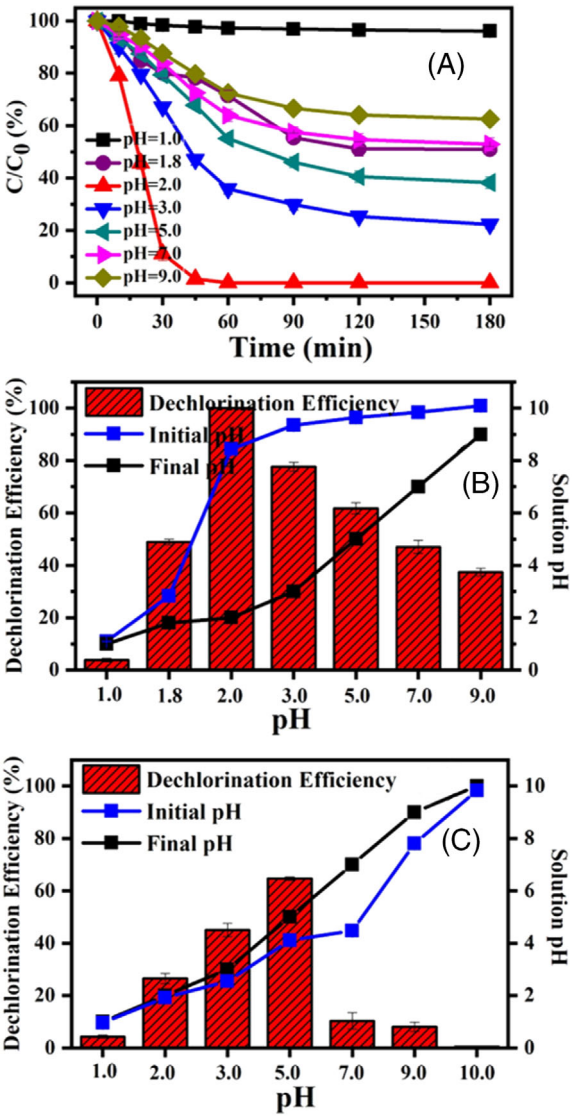

FIGURE 7 Catalytic activity of palladium nanoparticles (PdNPs) assemblies. Effects of solution pH on, A, the dechlorination of 4-chlorophenol (4-CP) with $NaBH_4$ as the hydrogen donor (C/C_0 indicates the ration between the concentrations of 4-CP at the given time and at $t = 0$) and, B, the final solution pH after $NaBH_4$ introduction. C, Effects of solution pH on the dechlorination of 4-CP, with H_2 as the hydrogen donor, and the solution pH. Reaction conditions: 25°C, 800 rpm, 1.0 mM 4-CP, 0.125 mM cetyltrimethylammonium bromide (CTAB), 15 mM $NaBH_4$ (or 2.23 mmol H_2), 12.5 mol% Pd (with respect to 4-CP)

2.3 | Influence of experimental parameters

The effects of the solution pH and the dosages of $NaBH_4$ and Pd on the dechlorination efficiency are useful to shed some light onto the catalytic process and explain the reasons why we ended up in choosing the specific concentrations and conditions of Figure 6.

2.3.1 | Effects of solution pH

The pH was varied from 1.0 to 9.0 by addition of a 1.0 M H_2SO_4 or NaOH solution. Figure 7 shows that upon

raising the pH the dechlorination performance first increases and then decreases. For example, after 3 hours the dechlorination efficiency is only about 4% at pH = 1.0, is quantitative at pH = 2.0, and then significantly decreases from about 78% (pH = 3.0) to 38% (pH = 9.0). This is attributed to the specific reaction conditions. Hydrolysis of $NaBH_4$ was used as the hydrogen source for the dechlorination of 4-CP. On the other hand, this hydrolysis depends on the pH: whereas acid-catalyzed hydrolysis takes place at low pH values, the hydrogen production rate is largely inhibited under alkaline conditions due to the coupled reaction $BH_4^- + 8OH^- \rightarrow BO_2^- + 6H_2O + 8e^-$.[52] Although the formation of H_2 by $NaBH_4$ hydrolysis is of great practical importance, it may result in the formation of the strongly basic metaborate ion ($B(OH)_4^-$), which gives rise to a sharp increase of the solution pH. As a matter of fact, Figure 7B illustrates that upon addition of 15 mM $NaBH_4$, the solution pH changes considerably from 1.0, 2.0, 3.0, 5.0, 7.0, and 9.0 to 1.10, 8.45, 9.35, 9.65, 9.85, and 10.10, respectively. It should be noted that the best dechlorination outcome for the reduction of organic chlorides on noble metal catalysts is achieved under weak acidic conditions.[31,32,34] As such, the significant increase in the solution pH is detrimental to the dechlorination performance. Because of the interplay between the solution pH and the $NaBH_4$ hydrolysis, distinct dechlorination outcomes in 4-CP reduction are thus observed at different initial pH conditions.

$NaBH_4$ plays the two important roles of providing the hydrogen source and affecting the pH. To gain more insights into the effect of pH on the dechlorination rate and, more importantly, test an alternative method to perform the dechlorination itself, we used H_2 instead of $NaBH_4$. Pure H_2 gas (50 mL, 2.23 mmol) was introduced into the 100 mL flask reactor, while keeping the pH and all other conditions constants. As expected, the catalytic activity of the PdNPs exhibits a strong pH dependence, with the dechlorination peaking at pH = 5.0 and a conversion of about 65% in 3 hours (Figure 7C). Larger or lower pH values are detrimental for the dechlorination process.

Interestingly, whereas the amounts of H_2 used directly or produced from $NaBH_4$ are almost the same, the maximum dechlorination outcomes are very different, that is, 65% in 3 hours vs 100% in 45 minutes, respectively. When $NaBH_4$ is used as the hydrogen donor, hydrogen originates from $NaBH_4$ or H_2O ($NaBH_4 + 2H_2O \rightarrow 4H_2 + NaBO_2$).[3] Pd can catalyze $NaBH_4$ hydrolysis and, hence, facilitate the hydrogen evolution reaction, a process in which palladium hydride is generated as an important intermediate.[3] Atomic hydrogen species are known to play a key role in dechlorination processes,[31] and consequently, the so-formed Pd-H could effectively contribute to convert 4-CP to phenol. Similarly, when hydrogen gas is used directly, a key step for the dechlorination is the dissociation of H_2 on the Pd surface. An important factor is thus the amount or pressure of H_2 in the system. Indeed, an increase of the amount of H_2 from 1.34 to 3.57 mmol increases the dechlorination efficiency from about 56% to 84% (in 3 hours), which indicates that, relative to the $NaBH_4$ promoted reaction, the poor dechlorination outcome is primarily due to the low dissolution of H_2 in the system. A better dechlorination performance of 4-CP might be attained under higher H_2 pressure conditions, which could provide an alternative for the versatile catalytic systems developed in this work to remove organic chloride pollutants.

2.3.2 | Effects of $NaBH_4$ dosage

The effect of the $NaBH_4$ concentration is illustrated in Figure 8A. As opposed to the direct use of H_2, the dechlorination efficiency does not increase constantly with an increase of the $NaBH_4$ dosage. The best dechlorination outcome (100% in 45 minutes) is observed at 15 mM concentration. Raising the dosage from 20 to 40 mM, the dechlorination performance undergoes a net decline from 76.1% to 36.2% in 60 minutes, suggesting that the role of $NaBH_4$ is not simply that of a hydrogen donor. Figure 8B shows the noticeable increase of the solution pH with the increase of the $NaBH_4$ concentration. As aforementioned, the solution pH plays a critical role for the dechlorination reaction. While addition of $NaBH_4$ affects the solution pH, the latter controls the hydrolysis of $NaBH_4$.[52] The $NaBH_4$ concentration is thus an important parameter in determining the reaction conditions, and consequently, the 4-CP dechlorination performance. The solution pH also determines the electrostatic/charged state of the species involved. For instance, under basic conditions, 4-CP forms 4-chlorophenolate anion.[53,54] This is beneficial for the migration of the latter to the cationic surfactant surface. On the other hand, hydroxide ions and the hydrolysis byproduct $B(OH)_4^-$ become competitive toward the sorption sites on the surfactant assemblies. Overall, it is this dual effect of $NaBH_4$ as a hydrogen source and on the solution pH that determines the final catalytic activity of PdNPs. The optimum concentration of 15 mM for $NaBH_4$ was thus chosen for the following experiments.

2.3.3 | Effects of Pd dosage

Regarding Pd, we investigated the catalytic activity of different PdNPs assemblies. The results were obtained for Pd dosages in the range of 1.0 to 20.0 mol% (with respect

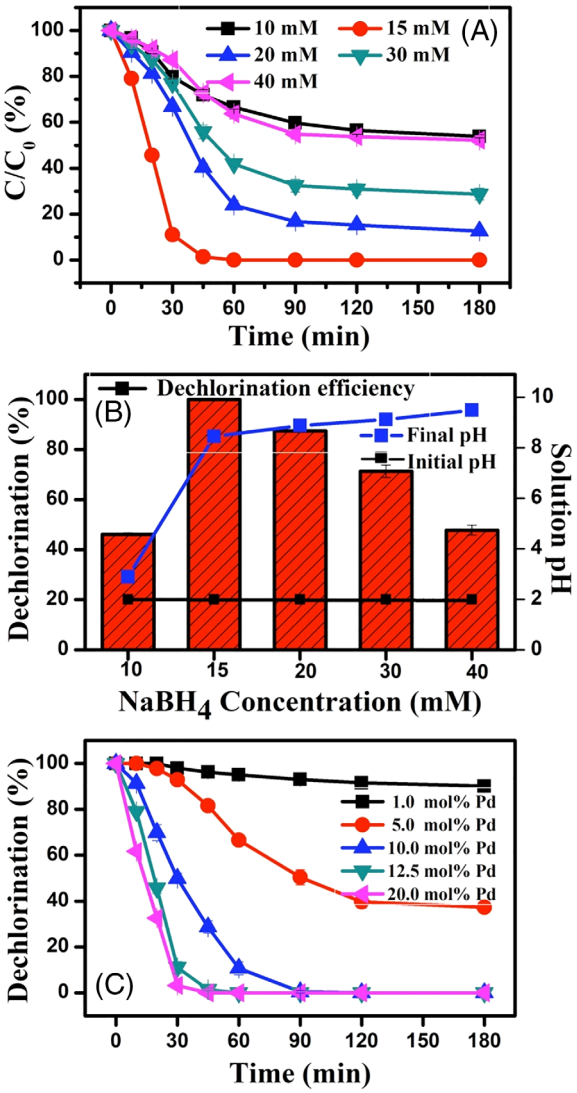

FIGURE 8 Catalytic activity of palladium nanoparticles (PdNPs) assemblies. A, Effects of $NaBH_4$ dosage concentration on the dechlorination of 4-chlorophenol (4-CP) (C/C_0 indicates the ration between the concentrations of 4-CP at the given time and at $t = 0$). B, Variations of dechlorination efficiency and solution pH with the introduction of $NaBH_4$ after 3 hours. C, Effects of Pd dosage amount on the dechlorination of 4-CP. Reaction conditions: pH 2.0, 25°C, 800 rpm, 1.0 mM 4-CP, 0.125 mM cetyltrimethylammonium bromide (CTAB), 15 mM $NaBH_4$, 12.5 mol% Pd (with respect to 4-CP)

to 4-CP). Figure 8C shows that there is a significant enhancement in dechlorination as the Pd dosage increases, whereas no dechlorination occurs in the absence of Pd. The dechlorination efficiency smoothly increases with the Pd dosage. In 60 minutes, for example, the efficiency is only 5.0% for the 1.0 mol% PdNPs assemblies, whereas it increases from 33.5% to 100% by increasing the amount of Pd from 5.0 to 12.5 mol%. At 20.0 mol % Pd dosage, complete dechlorination occurs in 30 minutes. As aforementioned, when the CTAB concentration is 0.125 mM (ie, lower than the CMC), a loose vesicle forms. On the other hand, retention of the ordered architecture formed by the CTAB-Pd precursors is critical for designing the specified PdNPs. During the making of the aggregate, addition of $NaBH_4$ causes the formation of the zero-valent PdNPs primarily at the hydrophilic region of the vesicle, where they aggregate and coalesce with each other to form layers on the outer and inner spheres of the vesicle. In this sense, the surfactant assembly could be seen as providing a template that imparts enough mechanical stability and dispersity to the so-formed PdNPs structure. As the Pd dosage increases, more catalytic activate sites are generated, thereby yielding a better dechlorination performance. However, due to the limited number of possible interactions between the cationic surfactant (at 0.125 mM) and Pd precursor, further increase in Pd dosage would result in the growth of the initially formed Pd crystals. Eventually, their size exceeds that of the volume of the vesicle with the effect of destroying the ordering of the surfactant assembly[2] and, consequently, impairing their catalytic activity. On these grounds, a moderate Pd dosage is deemed as essential to maintain the vesicle structure and keep the catalytic activity of PdNPs as high as possible. By considering the catalytic performance and the costly materials used, 12.5 mol% of Pd dosage was identified as the optimum dosage value.

2.4 | PdNPs-decorated nanoreactor for effective water remediation

2.4.1 | Simultaneous removal and in situ catalytic dechlorination of 4-CP for water remediation

A schematic illustration summarizing the process is shown in Figure 9. The CTAB molecules can form micelles spontaneously in aqueous solutions (Figure 9A). When the Pd precursor is added, formation the complex between the CTA^+ cations and $PdCl_4^{2-}$ takes place (Figure 9B). In this process exchange of Cl^- by Br^- occurs. The variation of the counterion may affect the shape, structure, and morphology of the formed micelles, and even cause the micelles to swell because of the now larger head group. Interaction with the Pd precursor has the effect of screening the repulsive forces between the CTA^+ head groups, thereby causing the CTAB micelles to reassemble into well-ordered architectures. Depending on the relative concentrations, vesicles, nanocubes, cylinders, spheres may form. Addition of $NaBH_4$ causes in situ formation of the PdNPs, which are generated and immobilized directly inside the ordered surfactant

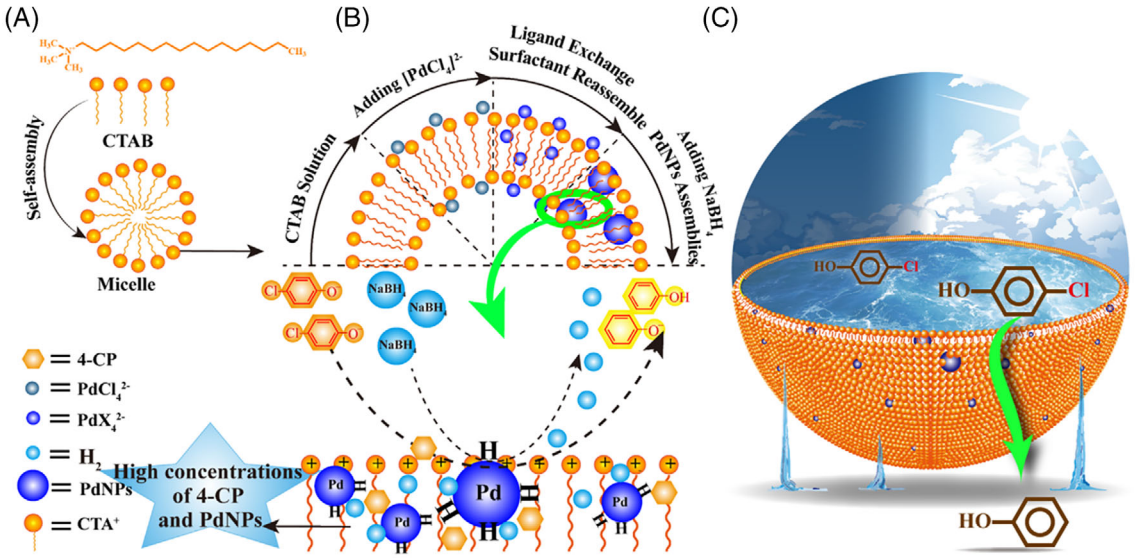

FIGURE 9 Schematic representation of palladium nanoparticles (PdNPs) assemblies formation. A, Cetyltrimethylammonium bromide (CTAB) micelle. B, Surfactant-directed assembly synthesis of PdNPs and the synergistic mechanism of excellent catalytic activity and stability of PdNPs assemblies for the dechlorination of 4-chlorophenol (4-CP). C, PdNPs assemblies as nanoreactors for water remediation

architecture. On these grounds, the making of tailor-made PdNPs assemblies can be successfully achieved. Overall, the surfactant plays a critical role in forming the well-ordered PdNPs-decorated assemblies, as it can effectively prevent aggregation of the PdNPs, and thereby, ensure good NPs dispersibility in the assemblies[55-57]; importantly, it also directs the formation of specific structures.

We now focus on the physiochemical property of the PdNPs assemblies and their environment implications as nanoreactors for effective water remediation. The PdNPs assemblies exhibit amphiphilic properties. The hydrophobic 4-CP can be solubilized by the hydrophobic tails of surfactant, also due to the p-π interaction between CTAB and 4-CP, as illustrated in Figure 9B. 4-CP thus behaves as a swelling agent for the assemblies, an effect that has been previously observed.[58,59] As a matter of fact, we observed that by increasing the dosage concentration of 4-CP from 0 to 8.0 mM, the particle size increases from 85.1 to 115.3 nm (dynamic light scattering experiments: see Supporting Information). In addition, the cationic head group of CTA^+ imparts the PdNPs assemblies some hydrophilic behavior. A high positive zeta potential (as high as 45 mV) was observed in the systems prepared (Supporting Information). Because of electrostatic interaction, the PdNPs assemblies thus display affinity also toward anionic species (eg, 4-chlorophenolate anion) and are very stable in water as a result of plenty of cationic head groups in the structures. The combination of these factors provides both hydrophilic and hydrophobic environments around the catalyst, which is beneficial for the removal of organic pollutants from aqueous solutions.

The proof-of-concept PdNPs-decorated nanoreactor indeed shows very promising features for water remediation. The Pd catalyst is indispensable for triggering hydrodechlorination due to its capability of forming atomic hydrogen species (H*).[60] In particular, the H_2 produced via hydrolysis of $NaBH_4$ can dissociate to form atomic hydrogen on the Pd catalyst surface; this species is adsorbed on the particles surface or even dermasorbed inside the Pd lattice. H* exhibits strong reduction capabilities and is highly efficient in the reductive cleavage of C—Cl bonds.[25,31-36] The ultrafine PdNPs here prepared with high stability and dispersity can concentrate and provide atomic hydrogen in large amount on the catalyst surface. As Figure 9B,C illustrates, these nanoreactors provide an environment that blends reductant (atomic hydrogen), pollutant target (4-CP), and Pd nanocatalyst surface, all in high concentration. The capability of concentrating hydrophobic substances and the rapid catalytic dechlorination promoted by the PdNPs are thus seen as key ingredients of the water remediation strategy proposed here. This is made possible by taking advantage of the amphiphilic and self-assembly properties of the surfactant, as well as the role of the latter in directing the preparation of effective heterogeneous catalysts.

2.4.2 | Catalysis stability and recyclability

The stability of a catalyst is an important parameter to consider. The recycle tests (Figure 10A) show that the

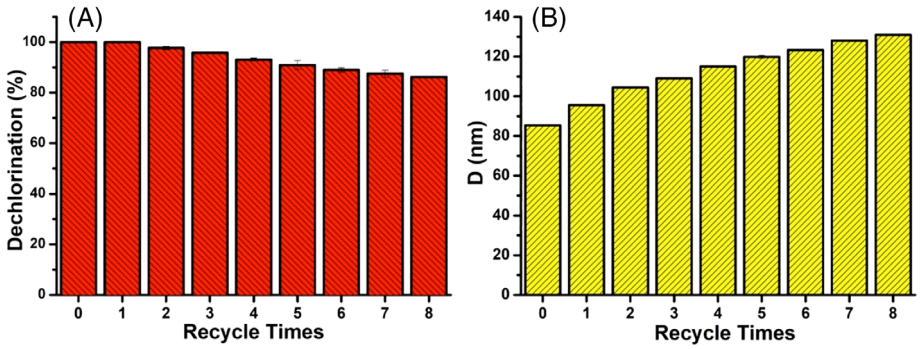

FIGURE 10 Stability of the palladium nanoparticles (PdNPs) assemblies. A, Recyclability of the PdNPs assemblies for the dechlorination of 4-chlorophenol (4-CP). B, Variation of the hydrodynamic radius of PdNPs assemblies with recycle times. Reaction conditions: pH = 2.0, 25°C, 800 rpm, 1.0 mM 4-CP, 0.125 mM cetyltrimethylammonium bromide (CTAB), 15 mM $NaBH_4$, 12.5 mol% Pd (with respect to 4-CP), 60 minutes

PdNPs assemblies exhibit an excellent dechlorination capacity and recyclability, as about 87% dechlorination efficiency (measured after 60 minutes) can still be achieved after eight-repeated treatments. We believe that this remarkable performance is due to the synergistic effect between surfactant assembly matrix and ultrafine PdNPs. In this context, it is worth mentioning that the TGA revealed that in the PdNPs assembly the total organics (surfactants) accounted for 33.1% of the total weight. The PdNPs recovered after the recycle tests were further characterized by TEM. The image in Figure S5 shows that PdNPs remained high dispersed, thereby indicating that no obvious aggregation phenomena occurred throughout the recycle experiments. This is keeping with the dechlorination results and further confirms the general stability of the Pd nanocatalysts (further details are provided in the Supporting Information). It should be noted that a small decline in dechlorination efficiency takes place, while a corresponding increase of the hydrodynamic radius of the PdNPs assemblies is observed, as shown in Figure 10B. It thus appears that the PdNPs assemblies gradually became larger after each treatment. Rather than in water, the reduction product, phenol, is better solubilized in the surfactant nanoenvironment; furthermore, the phenolate anions formed under alkaline conditions can be stabilized by the cationic surfactants via electrostatic attraction. These factors are seen as the main causes for the volume increase in the PdNPs assemblies. As to solubilities, in the hydrophobic surfactant environment and considering the dielectric-constant increase caused by the contribution of the charged heads, the pK_a values for 4-CP and the product phenol can be estimated from their DMF values, 17.3 and 18.8, respectively,[61] which indicates that the propensity of 4-CP to undergo dissociation is slightly more pronounced than for phenol. In addition, given the differences in their Kow (octanol-water partition coefficient) values (2.45 vs 1.46, respectively),[62] 4-CP exhibits a higher enrichment capacity than that of phenol in the PdNPs assemblies. These results further support the proof-of-concept nanoreactor where a substrates-rich microenvironment is created because of the surfactant property. Despite the slightly smaller solubility of phenol with respect to 4-CP, continuous accumulation of the product may progressively limit the dechlorination process, which to some extent could explain the decrease in dechlorination efficiency with the recycle times.

3 | CONCLUSION

We have described a dechlorination nanoreactor strategy based on the amphiphilic and self-assembling properties of the CTAB surfactant and the nanocatalytic properties of ultrafine PdNPs. The preparation of the nanoreactor, the effects of relevant parameters, the catalytic mechanism, and the test of the optimized catalyst in the dechlorination of a typical pollutant are presented and discussed. The surfactant-directed assembly of the PdNP-containing nanosystems could be controlled to yield loose vesicles, nanocubes, cylinders, and spherical assemblies. Formation of different structures is seen as determined by concentration-dependent electrostatic interaction between cationic surfactants and anionic Pd precursors. The resulting surfactant-stabilized systems contain highly concentrated ~5 nm PdNPs. These nanoreactors take advantage of the catalytic properties of the so-prepared PdNPs and provide hydrophobic regions that allow concentrating the target pollutant molecule and atomic hydrogen species. The results show that the so-devised catalytic approach exhibits a remarkable potential for the removal of organic chlorides, especially because of the rapid dechlorination ability, excellent catalytic activity, stability, and recyclability. This is the first example of

surfactant-directed assembly of metal NPs for the dechlorination of organic chlorides, and the first proposal of a nanoreactor strategy applied to water remediation.

4 | EXPERIMENTAL SECTION

4.1 | Chemicals

Palladium chloride was purchased from Kelong Chemical Reagent, Co., Ltd., China. 4-CP (>99.9%) was obtained from Sigma-Aldrich. The HPLC grade of methanol was purchased from Tedia Company Inc. Concentrated of 4-CP (10.0 mM) dissolved in water was prepared and used as a stock solution in the bath experiments. Analytical grade chemicals (CTAB, sodium borohydride ($NaBH_4$) and phenol) were purchased from Sinopharm Group Chemical Reagent, Co., Ltd., China. All these chemicals were directly used as received unless stated otherwise. Milli-Q water was used throughout the study with a resistivity of 18.2 MΩ.

4.2 | Synthesis of PdNPs assemblies

The PdNPs assemblies were prepared by a reduction method with $NaBH_4$ as a reductant. The whole experimental procedures were performed in a temperature-controlled water bath (25°C) under magnetic stirring (800 rpm). Briefly, 5.0 mL of aqueous solution containing 1.0 mM $PdCl_4^{2-}$ (pH = 1.0, adjusted by HCl solution) was mixed with 5.0 mL of a determined concentration of CTAB solution for half an hour. After that, 10 mL of $NaBH_4$ (5.0 mM) was added into the mixed solution dropwisely, and then the solution turned immediately to black as a consequence of the formation of zero-valent Pd particles (Equation (1)):

$$2PdCl_4^{2-} + BH_4^- + 3H_2O \rightarrow 2Pd^0 + H_2BO_3^- + 8Cl^- + 4H^+ + 2H_2 \quad (1)$$

The so-formed catalysts were directly used for the following dechlorination of 4-CP or characterization experiments.

4.3 | Catalysis tests

All the bath experiments for the dechlorination of 4-CP were carried out in a 100 mL three-necked flask reactor. A typical catalysis reaction was conducted as follows. After preparation of the PdNPs assemblies, a determined amount of 4-CP (0.04 mmol) was injected into the system together with around 14 mL of H_2O addition. Prior to each experiment, the solution pH was adjusted to the expected value by using 1.0 M H_2SO_4 or NaOH. The flask was then sealed with a butylene rubber stopper that was coated with Teflon. The catalysis reaction was initiated by spiking a certain amount of $NaBH_4$ into the flask now containing 40 mL of PdNPs suspension and 1.0 mM of 4-CP, which was performed under magnetic stirring and temperature-controlled (25°C, unless stated otherwise) conditions throughout the experiment. Aliquot of samples, filtrated by 0.22 μm membrane filter, were periodically withdrawn at determined time intervals during the catalysis test, which were immediately analyzed by HPLC. Triplicate experiments were carried out for each catalysis condition in order to ensure the accuracy of results, and the standard deviations were calculated correspondingly.

4.4 | Analytical methods

To obtain the surface morphologies and elemental compositions of the PdNPs assemblies, the latter were characterized with a TEM (JEM-3010, Japan, operated at 200 kV) coupled with EDS. The evolution of the surfactant-directed assembly synthesis of PdNPs was recorded in a full-wavelength scanning mode by UV-vis spectroscopy (Analytik Jena Specord 50 Plus, Germany), and the stability of the PdNPs assemblies was measured by spectrophotometric method in a drive-time mode with the wavelength fixing at 237 nm. The surface chemical compositions of the PdNPs assemblies were analyzed by XPS (Thermo ESCALAB 250XI) using a monochromatized Al Kα exciting radiation ($h\nu$ = 1486.6 eV) with a constant analyzer-pass energy of 40.0 eV. FTIR of the samples were recorded via KBr squash method using an ATR-FTIR spectrophotometer (Nicolet iz10, Thermo Fisher Scientific). The as-obtained PdNPs assemblies were subjected to TGA in nitrogen atmosphere (Thermal Gravimetric Analyzer, DTG-60AH, Shimadzu) with a gas flow rate of 50 mL min^{-1} and a heating rate of 10°C min^{-1}. The hydrodynamic radius and zeta potentials of the PdNPs assemblies were analyzed by Zetasizer Nano ZS90 (Malvern, UK). The concentrations of 4-CP and its dechlorination product phenol were determined by HPLC (Agilent 1100) equipped with a 4.6 mm × 150 mm, 5 μm Agilent ZORBAX Eclipse SB-C18. The mobile phase consisted of methanol and water with a ratio of 60:40 (vol:vol) at a flow rate of 1.0 mL min^{-1}. For all aqueous samples, the injection volume was 10 μL and quantification was carried out using a UV-vis detector set at 254 nm. Certified standards were

used for the identification and quantification of the substances based on the calibration curves.

ACKNOWLEDGMENTS

The authors gratefully acknowledge financial support from the National Natural Science Foundation of China (Nos. 5177091149, 51509021, and 51408209) and the Hunan Provincial Science and Technology Department (No. 2018SK2025).

CONFLICT OF INTEREST

The authors declare no conflict of interest.

ORCID

Binbin Huang https://orcid.org/0000-0001-6189-814X
Flavio Maran https://orcid.org/0000-0002-8627-6491

REFERENCES

1. Sheng T, Xu YF, Jiang YX, et al. Structure design and performance tuning of nanomaterials for electrochemical energy conversion and storage. *Acc Chem Res*. 2016;49:2569-2577.
2. Li C, Jiang B, Miyamoto N, Kim JH, Malgras V, Yamauchi Y. Surfactant-directed synthesis of mesoporous Pd films with perpendicular mesochannels as efficient electrocatalysts. *J Am Chem Soc*. 2015;137:11558-11561.
3. Huang B, Wang T, Lei C, Chen W, Zeng G, Maran F. Highly efficient and selective catalytic hydrogenation of acetylene in N,N-dimethylformamide at room temperature. *J Catal*. 2016;339:14-20.
4. Zhu Y, Fan L, Yang B, Du J. Multifunctional homopolymer vesicles for facile immobilization of gold nanoparticles and effective water remediation. *ACS Nano*. 2014;8:5022-5031.
5. Zhou Y, Zeng HC. Simultaneous synthesis and assembly of noble metal nanoclusters with variable micellar templates. *J Am Chem Soc*. 2014;136:13805-13817.
6. Jin R, Zeng C, Zhou M, Chen Y. Atomically precise colloidal metal nanoclusters and nanoparticles: fundamentals and opportunities. *Chem Rev*. 2016;116:10346-10413.
7. Bhattacharjee S, Basnet M, Tufenkji N, Ghoshal S. Effects of rhamnolipid and carboxymethylcellulose coatings on reactivity of palladium-doped nanoscale zerovalent iron particles. *Environ Sci Technol*. 2016;50:1812-1820.
8. Liu J, He K, Wu W, Song TB, Kanatzidis MG. In situ synthesis of highly dispersed and ultrafine metal nanoparticles from chalcogels. *J Am Chem Soc*. 2017;139:2900-2903.
9. Huang B, Qi C, Yang Z, et al. Pd/Fe3O4 nanocatalysts for highly effective and simultaneous removal of humic acids and Cr(VI) by electro-Fenton with H_2O_2 in-situ electro-generated on the catalyst surface. *J Catal*. 2017;352:337-350.
10. Vamvasakis I, Liu B, Armatas GS. Size effects of platinum nanoparticles in the photocatalytic hydrogen production over 3D mesoporous networks of CdS and Pt nanojunctions. *Adv Funct Mater*. 2016;26:8062-8071.
11. Yang H, Bradley SJ, Chan A, et al. Catalytically active bimetallic nanoparticles supported on porous carbon capsules derived from metal-organic framework composites. *J Am Chem Soc*. 2016;138:11872-11881.
12. Hu J, Yang Q, Yang L, et al. Confining noble metal (Pd, Au, Pt) nanoparticles in surfactant ionic liquids: active non-mercury catalysts for hydrochlorination of acetylene. *ACS Catal*. 2015;5:6724-6731.
13. Lu G, Li S, Guo Z, et al. Imparting functionality to a metal–organic framework material by controlled nanoparticle encapsulation. *Nature Chem*. 2012;4:310-316.
14. Liao CW, Lin YS, Chanda K, Song YF, Huang MH. Formation of diverse supercrystals from self-assembly of a variety of polyhedral gold nanocrystals. *J Am Chem Soc*. 2013;135:2684-2693.
15. Chiu CY, Chen CK, Chang CW, et al. Surfactant-directed fabrication of supercrystals from the assembly of polyhedral Au−Pd core−shell nanocrystals and their electrical and optical properties. *J Am Chem Soc*. 2015;137:2265-2275.
16. Yang CW, Chiu CY, Huang MH. Formation of free-standing supercrystals from the assembly of polyhedral gold nanocrystals by surfactant diffusion in the solution. *Chem Mater*. 2014;26:4882-4888.
17. Stein A, Rudisill SG, Petkovich ND. Perspective on the influence of interactions between hard and soft templates and precursors on morphology of hierarchically structured porous materials. *Chem Mater*. 2014;26:259-276.
18. Hu C, Lin K, Wang X, et al. Electrostatic self-assembling formation of Pd superlattice nanowires from surfactant-free ultrathin Pd nanosheets. *J Am Chem Soc*. 2014;136:12856-12859.
19. Owen J. The coordination chemistry of nanocrystal surfaces. *Science*. 2015;347:615-616.
20. Zhang ZC, Xu B, Wang X. Engineering nanointerfaces for nanocatalysis. *Chem Soc Rev*. 2014;43:7870-7886.
21. Albuquerque BL, Denicourt-Nowicki A, Mériadec C, Domingos JB, Roucoux A. Water soluble polymer–surfactant complexes-stabilized Pd(0) nanocatalysts: characterization and structure–activity relationships in biphasic hydrogenation of alkenes and a,b-unsaturated ketones. *J Catal*. 2016;340:144-153.
22. Naresh N, Wasim FGS, Ladewig BP, Neergat M. Removal of surfactant and capping agent from Pd nanocubes (Pd-NCs) using tert-butylamine: its effect on electrochemical characteristics. *J Mater Chem A*. 2013;1:8553-8559.
23. U.S. EPA. Priority pollutants. Appendix A to 40 CFR, Part 423. 1981. http://water.epa.gov/scitech/methods/cwa/pollutants.cfm.
24. Ministry of Environmental Protection of the People's Republic of China. *The Environmental Health Risk Directory for National Pollutants*. Beijing, China: China Environmental Science Press; 2009.
25. Wang X, Zhu M, Liu H, Ma J, Li F. Modification of Pd–Fe nanoparticles for catalytic dechlorination of 2,4-dichlorophenol. *Sci Total Environ*. 2013;449:157-167.
26. Kuleyin A. Removal of phenol and 4-chlorophenol by surfactant-modified natural zeolite. *J Hazard Mater*. 2007;144:307-315.
27. Lin CF, Wu CH, Onn ZN. Degradation of 4-chlorophenol in TiO2, WO3, SnO2, TiO2/WO3 and TiO2/SnO2 systems. *J Hazard Mater*. 2007;144:334-339.
28. Huang B, Durante C, Isee AA, Wei C, Gennaro A. Electrocatalytic properties of transition metals towards reductive dechlorination of polychloroethanes. *Electrochim Acta*. 2012;70:50-61.
29. Huang B, Long J, Chen W, Zhu Y, Zeng G, Lei C. Linear free energy relationships of electrochemical and thermodynamic parameters for the electrochemical reductive dechlorination of

chlorinated volatile organic compounds (Cl-VOCs). *Electrochim Acta*. 2016;208:195-201.
30. Huang B, Zhu Y, Li J, Zeng G, Lei C. Uncovering the intrinsic relationship of electrocatalysis and molecular electrochemistry for dissociative electron transfer to polychloroethanes at silver cathode. *Electrochim Acta*. 2017;231:590-600.
31. Huang B, Qian W, Yu C, Wang T, Zeng G, Lei C. Effective catalytic hydrodechlorination of o-, p- and m-chloronitrobenzenes over Ni/Fe nanoparticles: effects of experimental parameter and molecule structure on the reduction kinetics and mechanisms. *Chem Eng J*. 2016;306:607-618.
32. Xu J, Liu X, Lowry GV, et al. Dechlorination mechanism of 2,4-dichlorophenol by magnetic MWCNTs supported Pd/Fe nanohybrids: rapid adsorption, gradual dechlorination, and desorption of phenol. *ACS Appl Mater Interfaces*. 2016;8:7333-7342.
33. Cheng R, Wang JL, Zhang WX. Comparison of reductive dechlorination of p-chlorophenol using Fe0 and nanosized Fe0. *J Hazard Mater*. 2007;144:334-339.
34. Dong Z, Le X, Dong C, Zhang W, Li X, Ma J. Ni@Pd core–shell nanoparticles modified fibrous silica nanospheres as highly efficient and recoverable catalyst for reduction of 4-nitrophenol and hydrodechlorination of 4-chlorophenol. *Appl Catal B: Environ*. 2015;162:372-380.
35. Liu J, He F, Durham E, Zhao D, Roberts CB. Polysugar-stabilized Pd nanoparticles exhibiting high catalytic activities for hydrodechlorination of environmentally deleterious trichloroethylene. *Langmuir*. 2008;24:328-3336.
36. De CS, Hennebel T, Fitts JP, et al. Biosupported bimetallic Pd–Au nanocatalysts for dechlorination of environmental contaminants. *Environ Sci Technol*. 2011;45:8506-8513.
37. Yang B, Zhang Y, Deng S, et al. Reductive degradation of chlorinated organic pollutants-contaminated water by bimetallic Pd/Al nanoparticles: effect of acidic condition and surfactants. *Chem Eng J*. 2013;234:346-353.
38. Berhault G, Bausach M, Bisson L, Becerra L, Thomazeau C, Uzio D. Seed-mediated synthesis of Pd nanocrystals: factors influencing a kinetic- or thermodynamic-controlled growth regime. *J Phys Chem C*. 2007;111:5915-5925.
39. Sampedro B, Crespo P, Hernando A, et al. Ferromagnetism in fcc twinned 2.4 nm size Pd nanoparticles. *Phys Rev Lett*. 2003;91:237203.
40. Radowski MR, Shukla A, von Berlepsch H, et al. Supramolecular aggregates of dendritic multishell architectures as universal nanocarriers. *Angew Chem Int Ed*. 2007;46:1265-1269.
41. Hong HY, Mai YY, Zhou YF, Yan DY, Cui J. Self-assembly of large multimolecular micelles from hyperbranched star copolymers. *Macromol Rapid Commun*. 2007;28:591-596.
42. Zhou Y, Huang W, Liu J, Zhu X, Yan D. Self-assembly of hyperbranched polymers and its biomedical applications. *Adv Mater*. 2010;22:4567-4590.
43. Kajita S, Kohara S, Onodera Y, Fukunaga T, Matsubara E. Structural analysis of Pd-Cu-Si metallic glassy alloy thin films with varying glass transition temperature. *Mater Trans*. 2011;52:1349-1355.
44. Hosokawa S, Bérar JF, Boudet N, Ichitsubo T, Matsubara E, Nishiyama N. Local structure around Pd atoms in Pd42:5Ni7:5Cu30P20 excellent glass-former studied by anomalous X-ray scattering. *Mater Trans*. 2007;48:2358-2361.
45. Li W, Xiao F, Su H, Wang D, Yang X. Investigation of adsorption and photocatalytic activities of in situ cetyltrimethylammonium bromide-modified Bi/BiOCl heterojunction photocatalyst for organic contaminants removal. *RSC Adv*. 2016;6:93309-93317.
46. Alonso-Núñez G, Garza LM, Rogel-Hernández E, et al. New organometallic salts as precursors for the functionalization of carbon nanotubes with metallic nanoparticles. *J Nanopart Res*. 2011;13:3643-3656.
47. Santhanalakshmi J, Venkatesan P. Mono and bimetallic nanoparticles of gold, silver and palladium-catalyzed NADH oxidation-coupled reduction of eosin-Y. *J Nanopart Res*. 2011;13:479-490.
48. Upadhyay RK, Soin N, Saha S, Barman A, Roy SS. Fast and facile preparation of CTAB based gels and their applications in Au and Ag nanoparticles synthesis. *Mater Chem Phys*. 2015;156:105-112.
49. Gole A, Murphy CJ. Seed-mediated synthesis of gold nanorods: role of the size and nature of the seed. *Chem Mater*. 2004;16:3633-3640.
50. Gupta VKN, Mehra A, Thaokar R. Worm-like micelles as templates: formation of anisotropic silver halide nanoparticles. *Colloids Surf A: Physicochem Eng Aspects*. 2012;393:73-80.
51. Suia ZM, Chen X, Wang LY, et al. Capping effect of CTAB on positively charged Ag nanoparticles. *Physica E*. 2006;33:308-314.
52. Guella G, Zanchetta C, Patton B, Miotello A. New insights on the mechanism of palladium-catalyzed hydrolysis of sodium borohydride from 11B NMR measurements. *J Phys Chem B*. 2006;110:17024-17033.
53. Murray JW, Gordon NE. The dissociation constants of some chlorophenols. *J Am Chem Soc*. 1935;57:110-111.
54. Uchida M, Okuwak A. UV–vis spectrophotometric determination of the dissociation constants for monochlorophenols in aqueous solution at elevated temperatures. *J Solution Chem*. 2003;32:19-39.
55. Fan C, Bian T, Shang L, et al. pH-responsive reversible self-assembly of gold nanoparticles into nanovesicles. *Nanoscale*. 2016;8:3923-3925.
56. Shi R, Cao Y, Bao Y, et al. Self-assembled Au/CdSe nanocrystal clusters for plasmon-mediated photocatalytic hydrogen evolution. *Adv Mater*. 2017;29:1700803.
57. Shang L, Liang Y, Li M, et al. Naked magnetically recyclable mesoporous Au-gamma-Fe2O3 nanocrystal clusters: a highly integrated catalyst system. *Adv Funct Mater*. 2017;27:1606215.
58. Huang L, Kruk M. Versatile surfactant/swelling-agent template for synthesis of lLarge pore ordered mesoporous silicas and related hollow nanoparticles. *Chem Mater*. 2015;27:679-689.
59. Kruk M. Access to ultralarge-pore ordered mesoporous materials through selection of surfactant/swelling-agent micellar templates. *Acc Chem Res*. 2012;45:1678-1687.
60. Teschner D, Borsodi J, Wootsch A, et al. The roles of subsurface carbon and hydrogen in palladium-catalyzed alkyne hydrogenation. *Science*. 2008;320:86-89.
61. Maran F, Celadon D, Severin MG, Wanello E. Electrochemical determination of the pKa of weak acids in N,N-dimethy-l-formamide. *J Am Chem Sot*. 1991;113:9320-9329.
62. Kong L, Xiong Y, Sun L, et al. Sorption performance and mechanism of a sludge-derived char as porous carbon-based hybrid

adsorbent for benzene derivatives in aqueous solution. *J Hazard Mater*. 2014;274:205-211.

SUPPORTING INFORMATION

Additional supporting information may be found online in the Supporting Information section at the end of this article.

How to cite this article: Huang B, Xie Q, Yang Z, et al. Surfactant-directed Pd-nanoparticle assemblies as efficient nanoreactors for water remediation. *EcoMat*. 2020;1–15. https://doi.org/10.1002/eom2.12046